A R C H I V E S O F M E T A L L U R G Y A N D M A T E R I A L S
Volume 60 2015 Issue 2
DOI: 10.1515/amm-2015-0145

J. PARK*, K.H. JUNG**, G.A. LEE**, M. KAWASAKI***, B. AHN*,♯

# EVOLUTION OF PRECIPITATE MORPHOLOGY DURING EXTRUSION IN Mg ZK60A ALLOY

# EWOLUCJA MORFOLOGII WYDZIELEŃ PODCZAS WYTŁACZANIA STOPU Mg ZK60A

In this study, a continuously casted ZK60A magnesium alloy (Mg-Zn-Zr) was extruded in two different extrusion ratios, 6:1 and 10:1. The evolution of precipitates was investigated on the two extruded materials and compared with that of as-casted material. The microstructural analysis was performed by electron backscatter diffraction and transmission electron microscopy, and the compositional information was obtained using energy-dispersive X-ray spectroscopy. Several distinct morphologies of precipitates were observed, such as dot, rod, and disk shaped. The formation mechanisms of those precipitates were discussed with respect to the heat and strain during the extrusion process.

*Keywords*: magnesium alloy, ZK60A, precipitation, extrusion

## 1. Introduction

Recently, magnesium alloys have received great attention especially for the application of lightweight parts in the automotive and aerospace industries because of their excellent specific strength [1-4]. However, magnesium alloys currently have several drawbacks in properties that significantly limit the wide application in industries [5-7]. One of them is lower strength compared with that of commercial aluminum alloys, therefore magnesium alloys are often additionally processed by extrusion or forging at warm or hot temperatures to improve their strength. The precipitates generated during these forming processes also influence the strength.

Mg-Zn-Zr alloy system improves the mechanical properties through solid solution strengthening by Zn atoms in the matrix, and it can be further strengthened by formation of precipitates [8]. The sequence of precipitation formation in this alloy is in the order of supersaturated solid solution (SSSS), GP zones, $\beta\prime_1$ (rod shaped, metastable MgZn$\prime$), and $\beta\prime_2$ (disk shaped, stable MgZn) [8, 9]. The $\beta\prime_1$ precipitate is a transition phase, and the $\beta\prime_2$ precipitate is an equilibrium phase formed at relatively higher temperature and longer time than $\beta\prime_1$ formation [8]. In the present research, the evolution of precipitate morphologies depending on extrusion conditions was investigated, and the formation mechanism of $\beta\prime_1$ and $\beta\prime_2$ precipitates was discussed in detail.

## 2. Experimental

A commercial grade ZK60A (Mg-6 wt.% Zn-0.5 wt.% Zr) alloy was produced by semi-continuous casting and subsequently forward extruded at a ram speed of 1 mm/min. Two different extrusion ratios, 6:1 and 10:1, were employed at temperatures of 250°C and 350°C, respectively.

Microstructure of as-casted material and extruded materials was characterized using electron backscatter diffraction (EBSD), energy-dispersive X-ray spectroscopy (EDS), and transmission electron microscopy (TEM). For EBSD analysis, the materials were prepared using a precision ion beam polisher (Hitachi IM-3000) with 360 rotation holder at 3kV for 30 min. The grain structure was characterized using EBSD detector (EDAX DigiView-1 with TSL OIM software) in FE-SEM (Hitachi S4300SE). The EBSD scan areas were 400×650 $\mu$m$^2$ for as-casted material, 50×80 $\mu$m$^2$ for 6:1 extruded material, and 40×70 $\mu$m$^2$ for 10:1 extruded material. The in-plane step size of EBSD map was about 0.25 $\mu$m. After the raw orientation maps were collected, standard cleanup procedures were conducted to minimize the incorrectly indexed pixels and background noise. For TEM analysis, samples from bulk material were prepared by electrolytic jet polishing using a chemical solution primarily consisting of perchloric acid, citric acid, and ethanol at -7°C and 23 V. The TEM observation and compositional analysis were performed using a FE-TEM (FEI Tecnai G2) equipped with an EDS (EDAX).

## 3. Results and discussion

Fig. 1 shows EBSD results of as-casted, extruded (6:1), and extruded (10:1) materials, respectively. The as-casted material consists of primarily equiaxed grains with random crystallographic orientation and narrow size distribution as shown

* DEPARTMENT OF ENERGY SYSTEMS RESEARCH, AJOU UNIVERSITY, SUWON, KOREA
** METAL FORMING TECHNOLOGY R&BD GROUP, KOREAN INSTITUTE OF INDUSTRIAL TECHNOLOGY, INCHEON, KOREA
*** DIVISION OF MATERIALS SCIENCE AND ENGINEERING, HANYANG UNIVERSITY, SEOUL, KOREA
♯ Corresponding author: byungmin@ajou.ac.kr

in Fig. 1a. However, the grain structure of two extruded materials (6:1 and 10:1) appears to have coarse grains elongated along the extrusion direction and equiaxed fine grains, as shown in Fig. 1b and 1c respectively. Both coarse grains and ultrafine grains in two extruded materials exhibit preferred textures of (0001) or (2-1-10) planes parallel to the extrusion direction. Some fine grains were refined by large strain during the forward extrusion, and other very fine grains observed adjacent to elongated coarse grains were attributed to dynamic recrystallization. Therefore, the significant decrease in the average grain size stemmed from both grain refinements by large strain and dynamic recrystallization during the forward extrusion at elevated temperature.

Fig. 2 shows TEM micrographs from as-casted, 6:1 extruded, and 10:1 extruded materials. In all materials, two distinct morphologies of precipitates were observed: (i) disk shaped precipitates in a few hundred nanometer size observed mostly on the grain boundaries and (ii) dot shaped precipitates with very fine size of several nanometers distributed mostly within the grains. The disk shaped precipitates are preferentially formed at grain boundaries, because the self-diffusion coefficient at grain boundaries is generally higher than within the crystal which allows the solute atoms to rapidly migrate towards new nucleus positions within the grain boundary areas reducing high interfacial energy. Growth of these grain boundary precipitates involves the following steps: diffusion of atoms (i) to grain boundaries, (ii) along grain boundaries, and (iii) along precipitates interface accelerating thickening of precipitates [10].

TABLE 1 presents the elemental compositions of disk shaped precipitates from as-casted, 6:1 extruded, and 10:1 extruded materials measured using EDS in a scanning TEM (STEM) mode. For all three materials, the ratio of Zn to Mg contents in disk shaped precipitates is approximately 1:1 forming MgZn compound. Reportedly, the MgZn precipitates are formed as equilibrium $\beta\prime_2$ phase in over-aged conditions in Mg-Zn alloy system [8]. In general, very fine dot shaped precipitates evolve into rod shaped in uniaxial direction, then later into disk shaped in biaxial direction by diffusion of atoms from the matrix [10]. For the as-casted material, the disk shaped precipitates are predominant over the rod shape ones because of faster diffusion rate with higher mobility of atoms during solidification in the casting process which resembles artificial over-aging in terms of cooling profiles. Therefore, stable disk shaped precipitates were preferentially formed and grew at

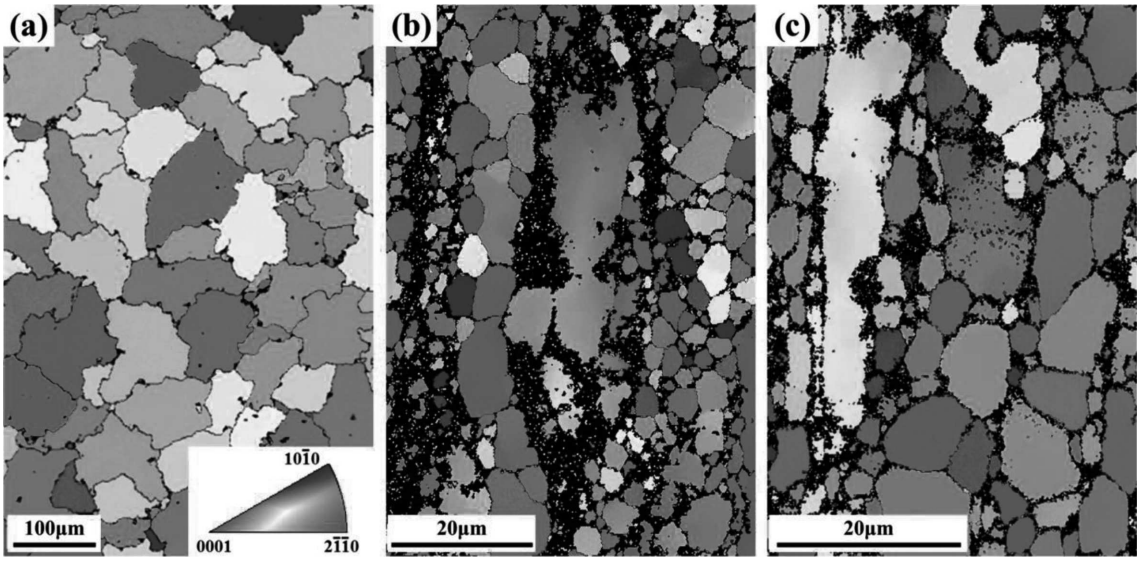


Fig. 1. EBSD inverse pole figure maps of (a) as-casted, (b) 6:1 extruded, and (c) 10:1 extruded materials

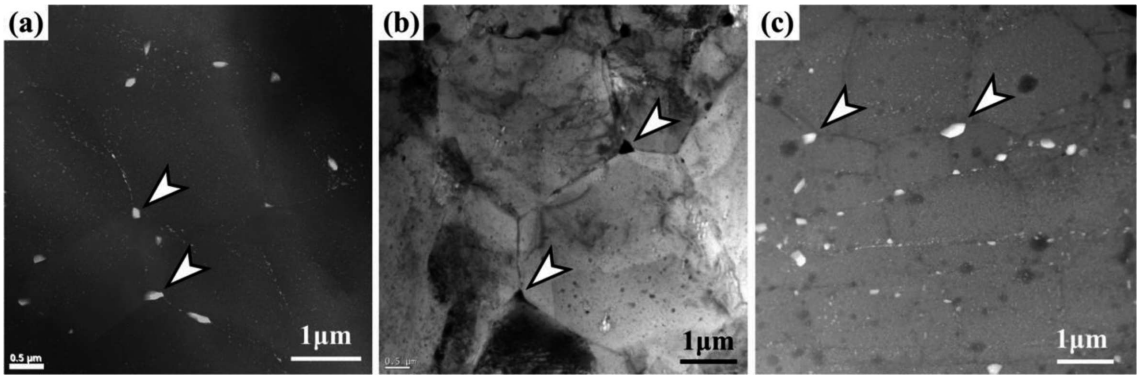


Fig. 2. TEM images of (a) as-casted, (b) 6:1 extruded, and (c) 10:1 extruded materials. The arrows indicate disk shaped precipitates

grain boundaries, and then the dot shaped fine precipitates were slowly formed within the grains at the latter part of solidification due to limited mobility of atoms.

TABLE 1
Chemical composition of disk shaped precipitates

| Element | As-casted (at.%) | 6:1 extruded (at.%) | 10:1 extruded (at.%) |
|---|---|---|---|
| Mg | 40.1 | 49.5 | 46.4 |
| Zn | 59.8 | 50.3 | 53.5 |
| Zr | 0.1 | 0.2 | 0.1 |

Fig. 3a and 3b show rod or needle shaped precipitates in the 6:1 extruded and 10:1 extruded materials, respectively. These rod shaped precipitates exist mostly within the grains which were not found in the as-casted material. This result indicates that the rod shaped precipitates in both extruded materials were apparently evolved from the dot shaped precipitates found in the as-casted material. Also, it was reported that similar rod shaped precipitates were formed as metastable $\beta\prime_1$ phase by age hardening [11, 12]. Therefore, it can be concluded that the extrusion temperature provided adequate thermal energy for dot shaped precipitates to evolve into the rod shaped ones which is equivalent to the thermal activation energy during regular aging process. However, none of the extruded materials contains disk shaped precipitates within the grains, because the thermal energy during the extrusion process was insufficient for further evolution to disk shaped precipitates.

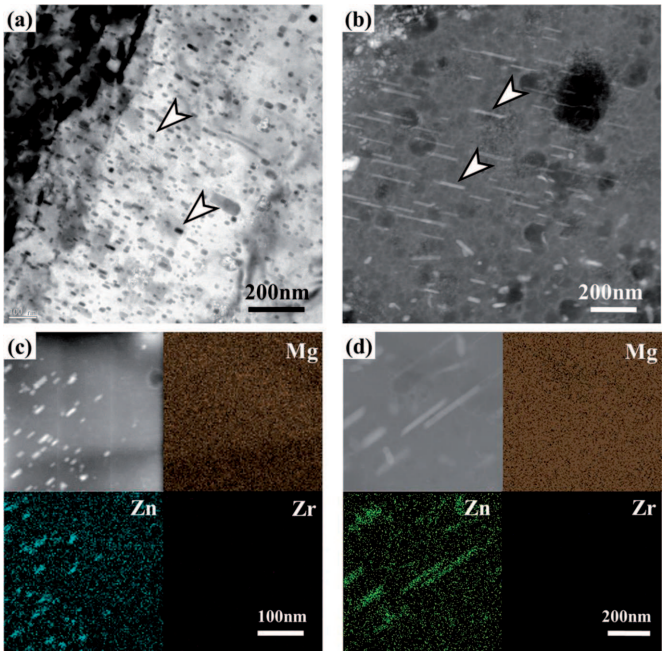


Fig. 3. TEM images and EDS elemental mappings of (a), (c) 6:1 extruded and (b), (d) 10:1 extruded materials, respectively. The arrows indicate rod shaped precipitates

As shown in Fig. 3a and 3b, the length of rod shaped precipitates in the 10:1 extruded material is apparently longer than that of the 6:1 extruded material. In the 6:1 extruded material, the length of precipitates is in the range of 40~50 nm in Fig. 3(a), while that of the 10:1 extruded material appears to be 150~200 nm in Fig. 3(b). This length variation is attributed to the difference of extrusion temperatures, 250 and 350°C, between two extrusion ratios, 6:1 and 10:1, respectively. In general, as extrusion ratio increases, extrusion process must be performed at higher temperatures in order to facilitate metal flow and to reduce friction with die. Also, when diffusion rate increases at higher temperatures, precipitates are lengthened by increase of its growth rate in the relationship given by Eq. 1 [10].

$$x \propto \sqrt{Dt} \tag{1}$$

where x is precipitate length, D is diffusion coefficient, and t is time. Eq. 1 indicates the length of precipitates is strongly dependent on temperatures because of positive correlation between diffusion coefficient and temperature. Therefore, the longer precipitates in the 10:1 extruded material stem from the higher extrusion temperature than the 6:1 extruded material.

Fig. 3c and 3d show the results of EDS elemental mapping for the 6:1 and 10:1 extruded materials, respectively. For both materials, the magnesium element exists in all areas without variation, while the X-ray intensity of zinc element was detected only from the precipitation areas. Virtually no zirconium element was measured by EDS elemental mapping because of the low contents in the ZK60A alloy.

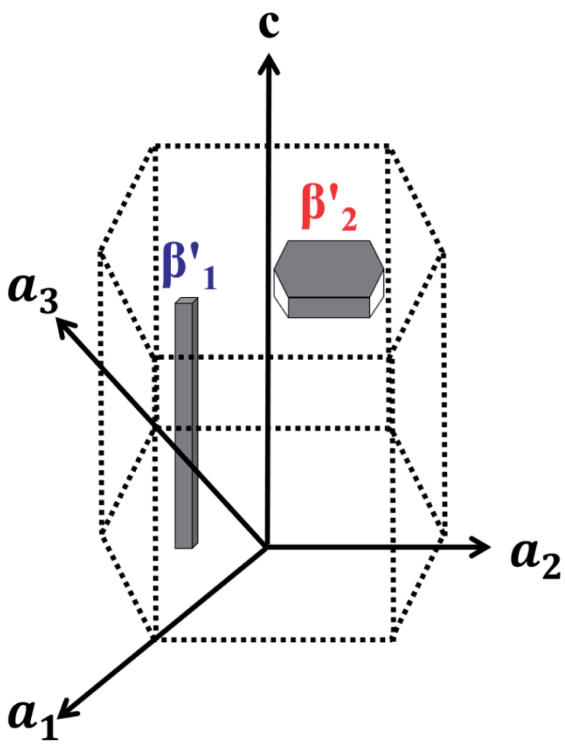


Fig. 4. Schematic representation of precipitation morphologies in $\beta_1'$, $\beta_2'$ phases [13]

Fig. 4 shows a schematic representation about preferential growth orientation of both rod and disk shaped precipitates in the hexagonal close packed (HCP) structure [13]. The rod shaped precipitates ($\beta_1'$) lie on the (11-20) planes and grow in the [0001] directions, whereas the disk shaped precipitates ($\beta_2'$) lie on the (0001) planes and grow any directions parallel to the (0001) planes [14]. Because the (0001) planes are primary slip planes in the HCP structure and parallel to the habit plane of

disk precipitates, dislocations can glide on the (0001) planes without strong interference by the disk precipitates. However, dislocation motions are significantly obstructed by the rod precipitates which lie and grow perpendicular to the (0001) gliding planes. Also, as discussed above, extrusion produces strong textures of (0001) or (2-1-10) planes parallel to the extrusion direction in Fig. 1b and 1c. For this reason, the rod shaped precipitates ($\beta_1'$) act as major impediments to the dislocation plasticity. Therefore, as a result, the 10:1 extrusion provides superior precipitation hardening effect than 6:1 extrusion, although not much variation of strain was applied by two different extrusion ratios.

## 4. Conclusions

In the present study, the precipitation behavior of extruded ZK60A magnesium alloy was investigated primarily using TEM analysis. Two distinct morphologies were found both in the as-casted material and the materials after extrusion, regardless of extrusion ratio. In the as-casted material, disk shaped precipitates were observed along grain boundaries while fine dot shaped precipitates were uniformly distributed within grains. After extrusion with two different extrusion ratios, the disk shaped precipitates remain in both extruded materials similar to those in as-casted material. The disk shaped precipitate is the stable equilibrium $\beta_2'$ phase (MgZn) so that they remain unchanged condition during the extrusion. However, two extruded materials with different extrusion ratios (6:1 and 10:1) exhibited rod shaped precipitates within grains which seem lengthened from the dot precipitates in as-casted alloy during extrusion process. The lengths of rod precipitates differ from each other in two extruded materials with different ratios. The longer precipitate in 10:1 extruded materials is attributed to higher extrusion temperature than 6:1 extruded material, because it is the metastable $\beta_1'$ phase (MgZn′). The rod shaped precipitates will affect the extent of precipitation hardening more than other precipitate morphologies, because they lie perpendicular to (0001) slip planes, and impede the movement of dislocations.

*Received: 20 November 2014.*

**Acknowledgements**

This research was supported by the Basic Science Research Program through the National Research Foundation of Korea (NRF) funded by the Ministry of Science, ICT & Future Planning (MSIP) of Korean government (Grant No. 2012R1A1A1012983). The authors would also like to acknowledge the financial support from the R&D Convergence Program of MSIP (Ministry of Science, ICT and Future Planning) and ISTK (Korea Research Council for Industrial Science and Technology) in the Republic of Korea (Grant No. B551179-11-02-00).

REFERENCES

[1] L. Wen, Z. Ji, X. Li, Materials Characterization **59**, 1655-1660 (2008).
[2] H. Yua, S.H. Park, B.S. You, Y.M. Kim, H.S. Yu, S.S. Park, Materials Science and Engineering A **583**, 25-35 (2013).
[3] X. Chen, F. Pan, J. Mao, J. Wang, D. Zhang, A. Tang, J. Peng, Materials and Design **32**, 1526-1530 (2011).
[4] X. Chen, X. Huang, F. Pan, A. Tang, J. Wang, D. Zhang, Transactions of Nonferrous Metals Society of China **21**, 754-760 (2011).
[5] T. Bhattacharjee, C.L. Mendis, T.T. Sasaki, T. Ohkubo, K. Hono, Scripta Materialia **67**, 967-970 (2012).
[6] W.J. Kim, I.K. Moon, S.H. Han, Materials Science and Engineering A **538**, 374-385 (2012).
[7] M. Thirumurugan, S. Kumaran, Transactions of Nonferrous Metals Society of China **23**, 1595-1601 (2013).
[8] D.K. Xu, L. Liu, Y.B. Xu, E.H. Han, Materials Science and Engineering A **420**, 322-332 (2006).
[9] J. Buha, Materials Science and Engineering A **492**, 11-19 (2008).
[10] D.A. Porter, K.E. Easterling, M. Sherif, Phase transformations in metals and alloys, CRC Press, Florida (1981).
[11] M. Paramsothy, M. Gupta, Journal of Alloys and Compounds **580**, 604-610 (2013).
[12] H. Chen, S.B. Kang, H. Yu, J. Cho, H.W. Kim, G. Min, Journal of Alloys and compounds **476**, 324 -328 (2009).
[13] C.J. Bettles, M.A. Gibson, K. Venkatesan, Scripta Materialia **51**, 193-197 (2004).
[14] X. Gao, J.F. Nie, Scripta Materialia **56**, 645-648 (2007).